

Supporting Information

**Tailoring the Ethanol Selectivity of SnO<sub>2</sub>-based MEMS Gas Sensors via WO<sub>3</sub>-loading in Double-Pulse-Driven Mode**

Tao Ren,<sup>a</sup> Koichi Suematsu,<sup>\*b</sup> Yusuke Shimada,<sup>b</sup> Yusuke Inomata,<sup>c</sup> Tetsuya Kida,<sup>d</sup> Ken Watanabe,<sup>b</sup> and Kengo Shimano<sup>e\*</sup>

<sup>a</sup> *Interdisciplinary Graduate School of Engineering Sciences, Kyushu University, Kasuga, Fukuoka 816-8580, Japan.*

<sup>b</sup> *Department of Advanced Materials Science and Engineering, Faculty of Engineering Sciences, Kyushu University, Kasuga, Fukuoka 816-8580, Japan.*

<sup>c</sup> *Faculty of Advanced Science and Technology, Kumamoto University, Kumamoto, 860-8555, Japan.*

<sup>d</sup> *Kumamoto University, Institute of Industrial Nanomaterials (IINa), Kumamoto, 860-8555, Japan.*

Corresponding author e-mail address: suematsu.koichi.682@m.kyushu-u.ac.jp, shimanoe.kengo.695@m.kyushu-u.ac.jp

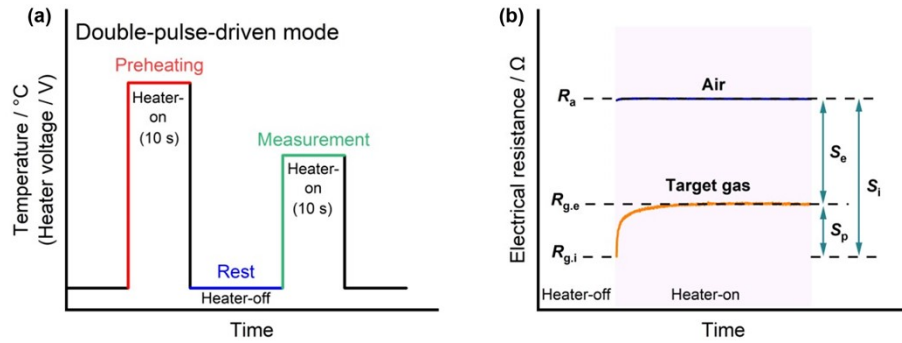


**Fig. S1.** (a) schematic of heater voltage and temperature profiles during double-pulse driven operation. (b) Definition of the sensor response.

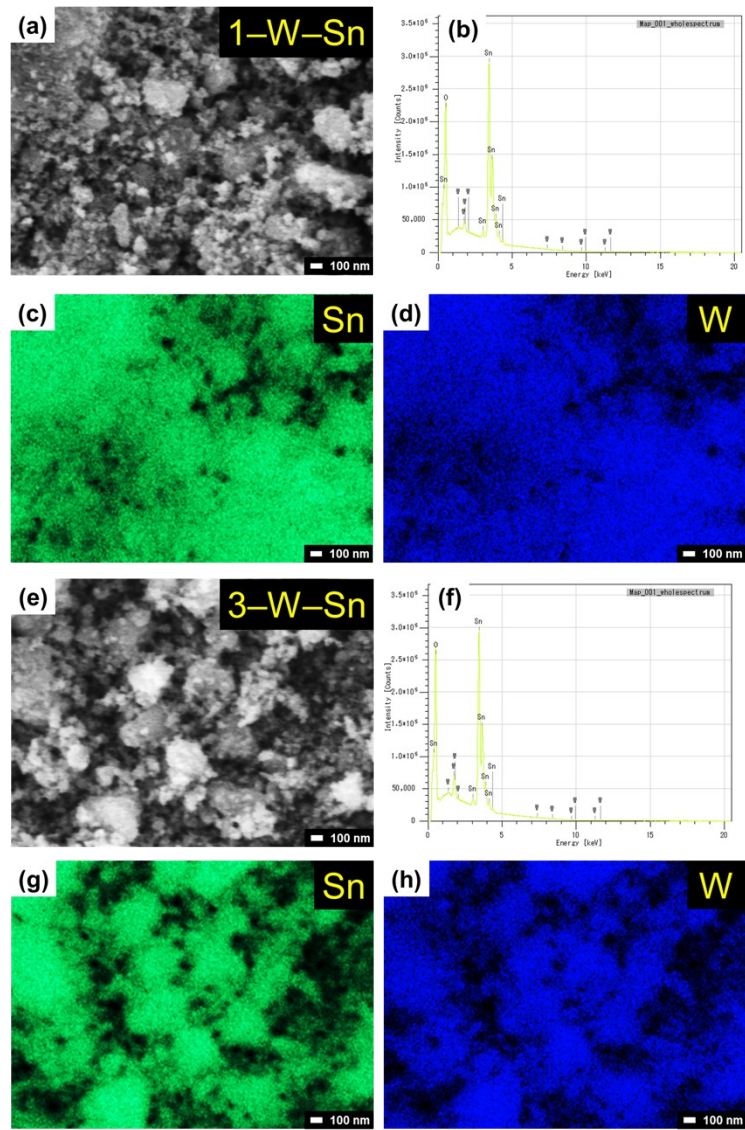


**Fig. S2.** Morphological and compositional analysis of (a–d) 1–W–Sn, and (e–h) 3–W–Sn sample.

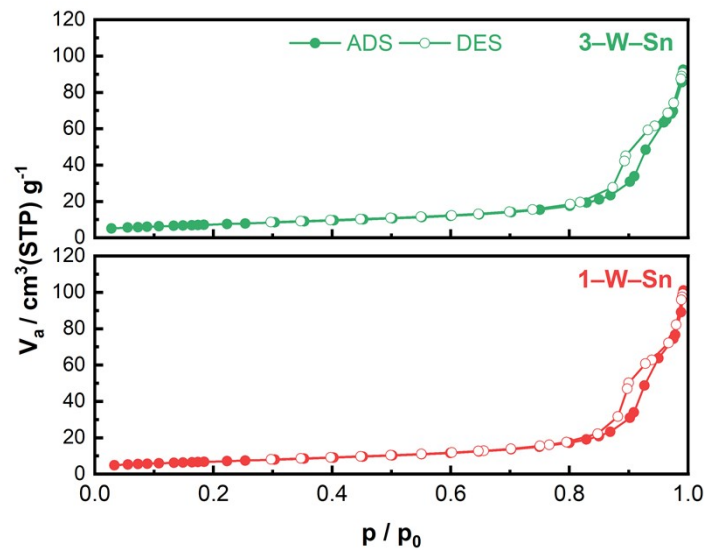


**Fig. S3.**  $\text{N}_2$  adsorption-desorption isotherms of 1-W-Sn and 3-W-Sn sample.

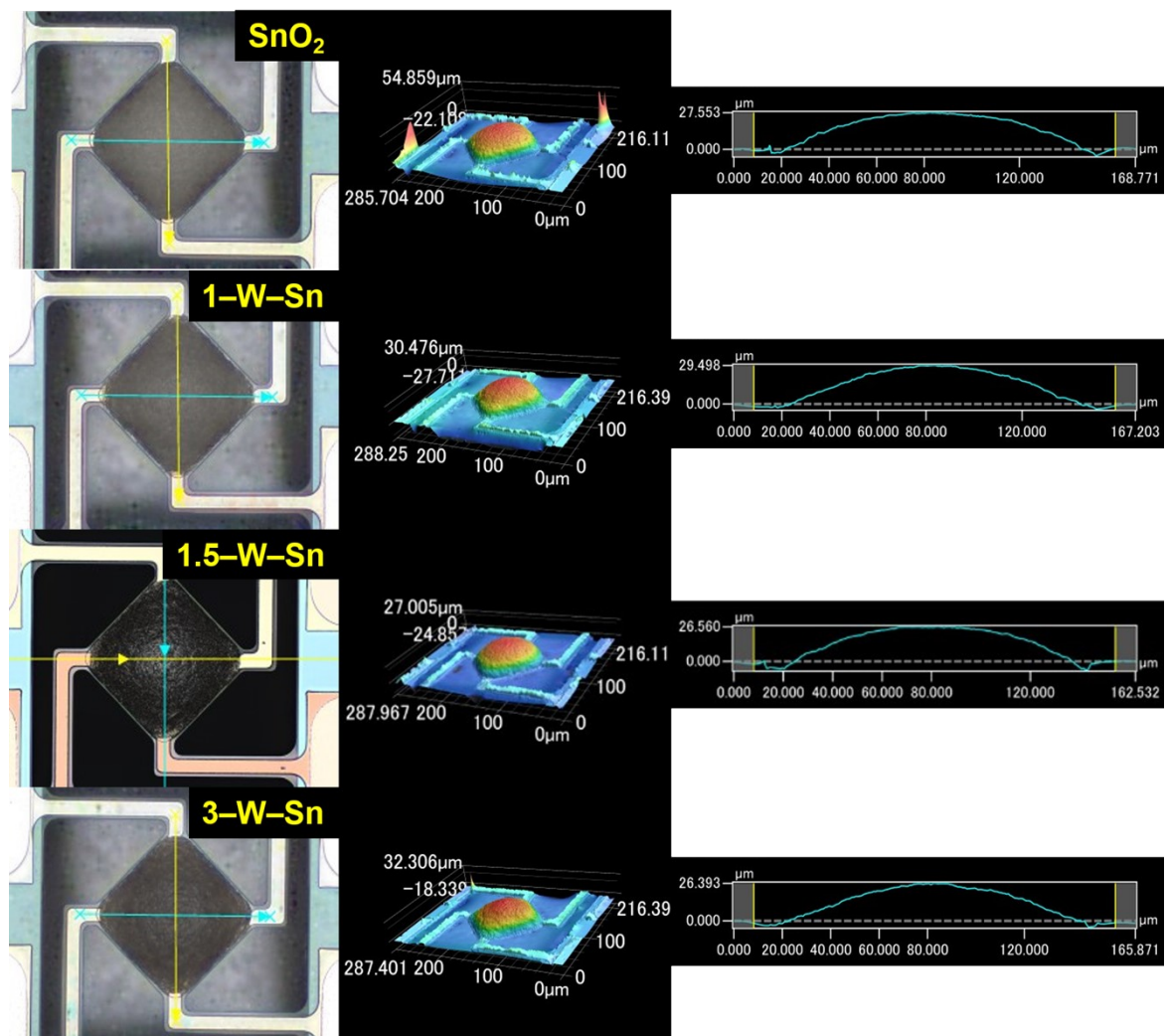


**Fig. S4.** The physical morphology and film thickness of the fabricated MEMS sensor devices.

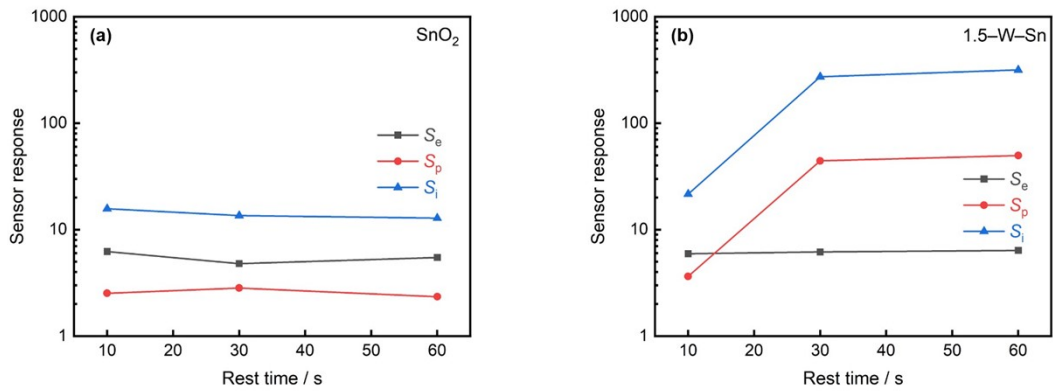


**Fig. S5.** Rest time dependence of the sensor response for the (a)  $\text{SnO}_2$  and (b) 1.5-W-Sn sensors to 10 ppm ethanol at measurement temperature of 350 °C.

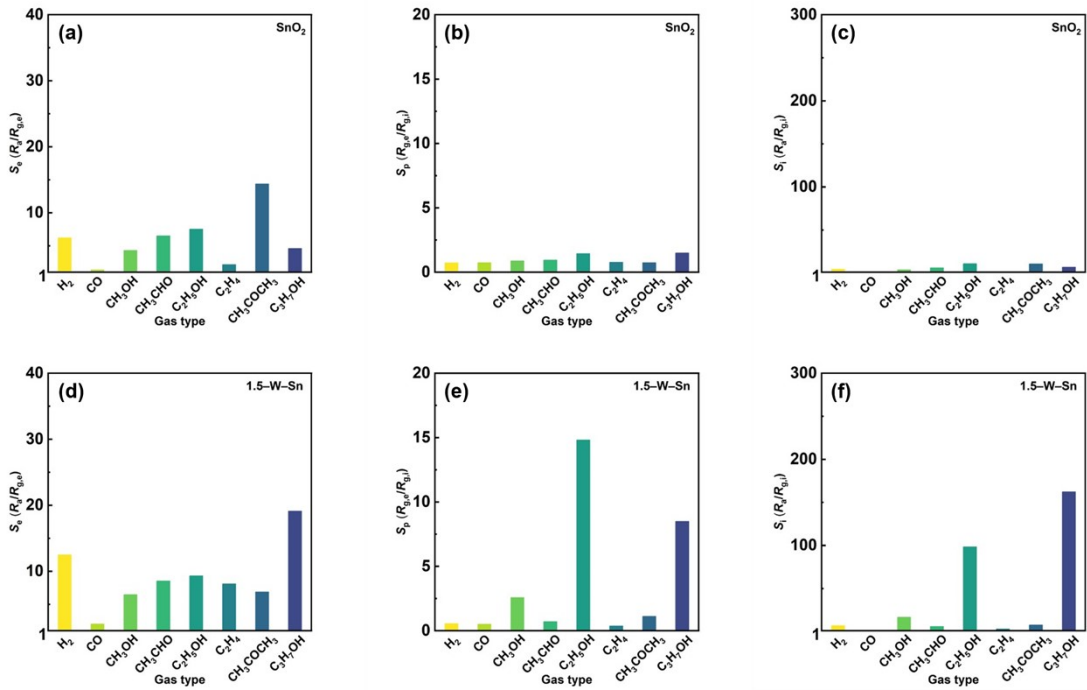


**Fig. S6.** The sensor responses ( $S_e$ ,  $S_p$  and  $S_i$ ) of fabricated MEMS sensors containing (a-c)  $\text{SnO}_2$ , and (d-f) 1.5-W-Sn to 10 ppm various target gases at measurement temperature of 300 °C.

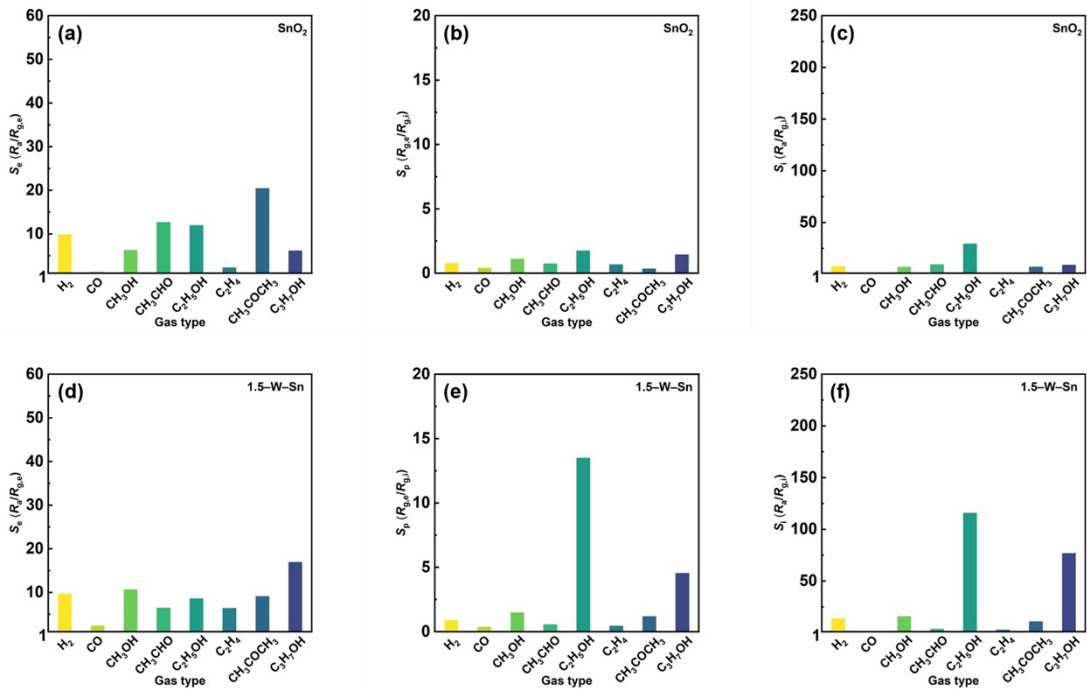


**Fig. S7.** The sensor responses ( $S_e$ ,  $S_p$  and  $S_i$ ) of sensors containing (a-c)  $\text{SnO}_2$ , and (d-f) 1.5-W-Sn to 10 ppm various target gases at measurement temperature of 250 °C.

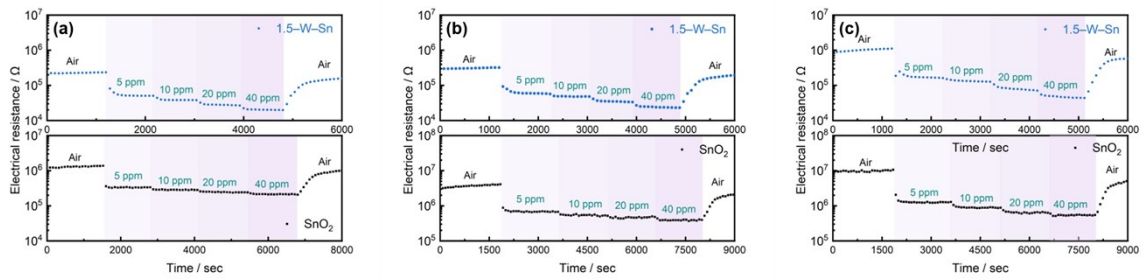


**Fig. S8.** Dynamic response curves of sensors containing neat  $\text{SnO}_2$  and 1.5–W–Sn to ethanol at (a) 350  $^{\circ}\text{C}$ , (b) 300  $^{\circ}\text{C}$  and (c) 250  $^{\circ}\text{C}$ .

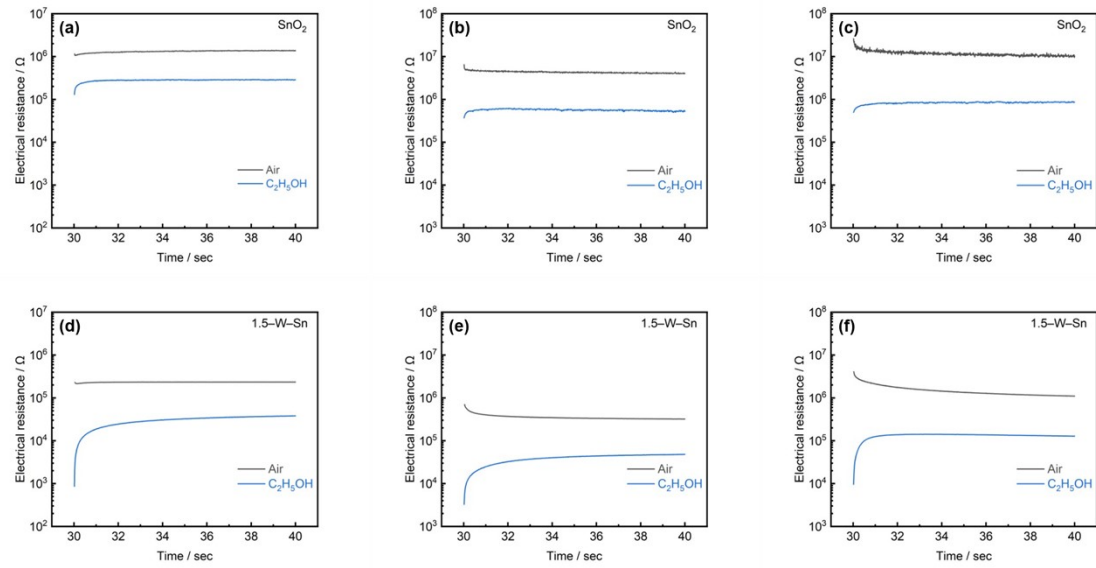


**Fig. S9.** The electric resistance curves in synthetic air and 10 ppm ethanol/air during a pulse heating step at 350, 300 and 250 °C under double-pulse-driven mode using (a–c) SnO<sub>2</sub>, (d–f) 1.5–W–Sn, respectively.

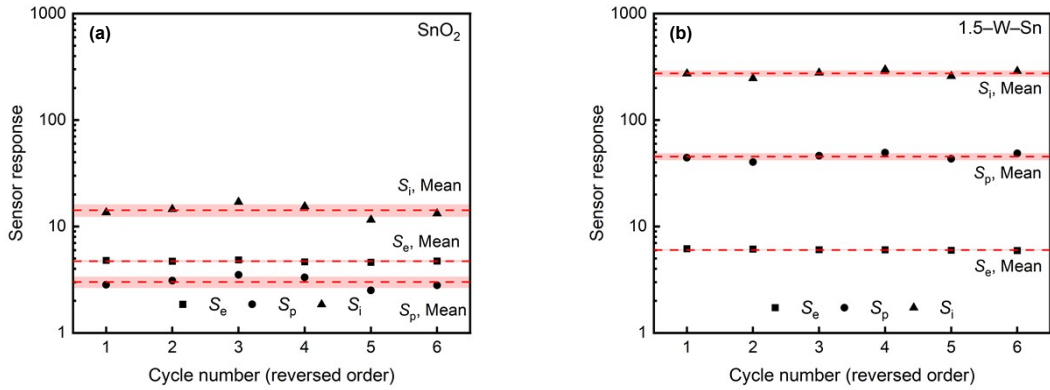


**Fig. S10.** Stability of the sensor response for the (a)  $\text{SnO}_2$  and (b) 1.5–W–Sn sensors to 10 ppm ethanol at measurement temperature of 350 °C under DP mode.

Stability of the sensor responses ( $S_e$ ,  $S_p$ , and  $S_i$ ) for (a) neat  $\text{SnO}_2$  and (b) 1.5–W–Sn sensors toward 10 ppm ethanol at a measurement temperature of 350 °C under DP mode was shown in Fig. S10. The data points represent the responses from 6 representative consecutive cycles. The dashed red lines indicate the mean value for each response parameter. The Relative Standard Deviation values for 1.5–W–Sn were calculated to be 1.4% ( $S_e$ ), 7.5% ( $S_p$ ), and 6.9% ( $S_i$ ).